Evaluation of Bone-Tendon Junction Healing Using Water Jet Ultrasound Indentation Method

Min-Hua LU[1,3], Yong-Ping ZHENG [1,2], Hong-Bin LU[4], Qing-Hua HUANG [1,5], Ling QIN[4]

[1] Department of Health Technology and Informatics, [2] Research Institute of Innovative Products and Technologies, The Hong Kong Polytechnic University, Hung Hom, Hong Kong, China.

[3] Department of Biomedical Engineering, Shen Zhen University, Guangdong Province, China

[4] Muscular-Skeletal Research Laboratory, Department of Orthopaedics & Traumatology, The Chinese University of Hong Kong, Shatin, N.T. Hong Kong, China

[5] School of Electronic and Information Engineering, South China University of Technology, Guangzhou, China

Corresponding author:
Yongping Zheng
Department of Health Technology and Informatics,
The Hong Kong Polytechnic University,
Hung Hom, Kowloon, Hong Kong SAR, P. R. China.
Tel: 852-27667664
Fax: 852-23624365
Email: ypzheng@ieee.org

Submitted to: Ultrasound in Medicine and Biology
First submission: May 24 2008

Abstract

The re-establishment of bone-tendon junction (BTJ) tissues with the junction, characterized as a unique transitional fibrocartilage zone, is involved in many trauma and reconstructive surgeries. Experimental and clinical findings have shown that a direct BTJ repair requires a long period of immobilization which may be associated with a postoperative weak knee. Therefore, it's very necessary to evaluate the morphological and mechanical properties of BTJ tissues *in situ* to better understand the healing process for the purpose of reducing the adverse effects of immobilization. We previously reported a noncontact ultrasound water jet indentation system for measuring and mapping tissue mechanical properties. The key idea was to utilize a water jet as an indenter as well as the coupling medium for high-frequency ultrasound. In this paper, we used the ultrasound water jet indentation to evaluate the BTJ healing process. The system's capability of measuring the material elastic modulus was first validated using tissue-mimicking phantoms. Then it was employed to assess the healing of the BTJ tissues after partial patellectomy over time on twelve 18-week-old female New Zealand White rabbits. It was found that, in comparison with the normal control samples, the elastic modulus of the fibrocartilage of the postoperative samples was significantly smaller, while its thickness increased significantly. Among the postoperative sample groups, the elastic modulus of the fibrocartilage of the samples harvested at week 18 was significantly higher than those harvested at week 6 and week 12, which was even comparable with the value of the control samples at the same sacrificed time. The results suggested that the noncontact ultrasound water jet indentation system provided a nondestructive way to evaluate the

material properties of small animal tissues *in situ*, thus had the ability to evaluate the healing process of BTJ.

Keywords: ultrasound, indentation, ultrasound indentation, water jet, bone-to-tendon junction repair, articular cartilage, soft tissue, elasticity.

Introduction

Many trauma and reconstructive surgeries involve re-establishment of the bone-tendon junction (BTJ) tissues. BTJ, such as patellar tendon-patella junction, is characterized with a unique transitional fibrocartilage zone, with calcified fibrocartilage connecting to bone and non-calcified fibrocartilage connecting to tendon (Benjamin et al 1998, Gao and Messner 1996, Woo 1987). Injuries to the BTJ often occur in the hand, foot, knee, ankle and shoulder because of trauma and sports injuries related to overloading or chronic stress disorders. Partial patellectomy with repair of the extensor mechanism to the remaining patella using various fixation techniques is clinically indicated for severe comminuted fractures or transverse fractures (Hung et al 1993, Saltzman et al 1990). Radiological observation demonstrated a significant increase in length of the remaining patella of patients from the preoperative stage up to 5 years postoperatively (Saltzman et al 1990), which was confirmed as new bone formation at the BTJ healing interface experimentally (Lu et al 2006, Qin et al 1999a, 2006a). Histologically, the metaplasia of the scar tissue observed next to the healing interface of the remaining patellar articular cartilage and the outgrowth of trabecular bone from the remaining patella with healing over time may increase the articular surface of the remaining patella after partial patellectomy (Qin et al 1999a). The BTJ healing takes place between two different tissues, and the regeneration of the junctional fibrocartilage zone has been found to be slow and difficult in both clinical and experimental studies (Nebelung et al 2003, Leung et al 2002). Therefore, it requires a longer resting and immobilization period before limb loading activities are permitted. However, the negative effects of longer immobilization on the healing tissue and other involved tissues are well known, including muscle and tendon

78 atrophy, bone loss and articular cartilage degeneration (Buckwalter 1995, 1996, Burr et al
79 1984, Fu et al 1998, Leung et al 1999, Qin et al 1997, Woo et al 1982, 1987). Hence, it's
80 very important to assess the mechanical properties of the BTJ tissues *in situ* or *in vivo* as
81 an evaluation of the healing so as to monitor the healing process, and to reduce the
82 adverse effects of immobilization.

83 Indentation is a widely used technique to measure the mechanical properties of
84 soft tissue, especially the compressive properties because it does not require special
85 preparation for the specimens and can determine the material properties of soft tissues *in*
86 *situ* or *in vivo*. Theoretical analysis of general indentation problems with various
87 idealizations of the physical model has been conducted for about a century and some
88 mathematical solutions have been reported for thin-layer soft tissues and materials using
89 different mechanical models (Waters 1965, Hayes et al 1972, Mak et al 1987, Mow et al
90 1989, Yu and Blanchard 1996, Sakamoto et al 1996, Haider and Holmes 1997). To
91 perform indentation on soft tissues, especially on articular cartilage, a number of
92 mechanical, arthroscopic and ultrasound indentation instruments have been developed.
93 Mechanical indentation instruments usually use a rigid stainless-steel indenter to deform
94 the sample, and employ a linear variable differential transducer (LVDT) to monitor the
95 indentation depth and a load cell to record the indentation force (Kempson et al 1971,
96 Hori and Mockros 1976, Mow et al 1989, Newton et al 1997, Arokoski et al 1994, 1999,
97 Athanasiou et al 1995, 1999, Shepherd and Seedhom 1997). The mechanical indentation
98 instruments can provide accurate and repeatable indentation measurements, but their
99 structures are normally bulky and complicated. Therefore, they are not convenient for *in*
100 *vivo* measurement of body tissues. In addition, as some mechanical instruments employ a

101 needle probe to penetrate into the cartilage to measure the tissue thickness which is
102 important information for the estimation of elastic modulus (Jurvelin et al 1990, Suh and
103 Spilker 1994, Zhang et al 1997, Yang 2003), destruction of the tissue structure might be
104 caused. Arthroscopic indentation apparatuses can perform experiments *in vivo* (Lyyra et
105 al 1995, Neiderauer et al 1998, Neiderauer et al 2004), however, they can't measure the
106 tissue thickness thus difficult to provide the accurate elastic modulus of cartilage.

107 During recent decades, ultrasound techniques together with compression or
108 indentation have successfully been used for the measurement (Wilson and Robinson 1982,
109 Zheng and Mak 1996, Hsu et al 1998, Adam et al 1998, Suh et al 2001, Kawchuk et al
110 2000, Laasanen et al 2002) or imaging (Ophir et al 1991, 1997, Gao et al 1996, Wilson et
111 al 2000, Han et al 2003, Greenleaf et al 2003, Svensson and Amiras 2006) of the
112 mechanical properties of soft tissues. The basic principle is to compress soft tissue using
113 an ultrasound transducer or the transducer/compressor combination, and collect the
114 ultrasound echoes before and after the compression. By analyzing the pairs of echoes
115 scattered from tissues to obtain the displacements of tissues at different sites, the local
116 strain distribution or the overall deformation of the compressed tissues can be obtained.
117 The accuracy of ultrasonically measured displacement during indentation has been earlier
118 investigated (Zheng and Mak 1996, Kawchuk and Elliott 1998, Kawchuk et al 2000,
119 Jurvelin et al 1995, Adam et al 1998, Appleyard et al 2001, Suh et al 2001), and
120 researchers concluded that the accuracy of ultrasound in measurement of tissue thickness
121 and displacement is highly similar with that of CT and other conventional techniques. As
122 ultrasound indentation can simultaneously measure the tissue thickness and deformation
123 non-invasively and is easy to use for *in vivo* stiffness measurement, it has been widely

used for assessment of normal limb tissues (Zheng and Mak 1999), residual limb tissues (Zheng et al 1999), diabetic foot tissue (Zheng et al 2000a, Hsu et al 2000), fibrotic neck tissue induced by radiotherapy (Zheng et al 2000b, Leung et al 2002, Huang et al. 2006), breast tissue (Yu et al. 2006), carpal tunnel tissue (Zheng et al. 2006), spinal tissues (Kawchuk et al 2001), and articular cartilage (Suh et al 2001, Laasanen et al 2003).

Present ultrasound indentation techniques utilize an unfocused transducer as the indenter to compress the soft tissue. Direct contact between the transducer and the specimen makes it difficult for them to properly compress small tissue specimens, such as the articular cartilage of rabbits due to the relatively large size of the transducer, and may also cause potential tissue damage. Therefore, a measurement device which may avoid contact and use very low loading forces is desirable to quantify the stiffness of soft tissues. We have earlier reported the development of a noncontact ultrasound indentation system that was capable of determining the material properties of soft tissues without a direct contact between the testing probe and soft tissues (Lu et al 2005, 2006). The key idea was to use a water jet as the indenter and simultaneously as the coupling medium for ultrasound to propagate through. By analyzing the response of soft tissues to water jet loading and the ultrasound echoes reflected from the tissues, the mechanical properties of soft tissues could be obtained. The non-contact nature enables the system to provide not only quantitative measurement of the tissue elastic properties, but also convenient scan over the tissue surface to map the distribution of the mechanical properties.

In this study, the capability of the system to map the elastic properties was first verified using tissue-mimicking phantoms, then the performance of the ultrasound water jet indentation system in assessing the healing of BTJ tissues of rabbits after partial

patellectomy was tested, and the results were compared with those obtained from histological analysis.

Materials and methods

Animal model and surgery

Twelve female New Zealand White rabbits (age:18-week-old, and weight: 3.5±0.3 kg) were prepared and randomly divided into 3 groups. The standard partial patellectomy and surgical reconstruction between the patella and patellar tendon were applied to the rabbits using a previously established protocol (Qin et al 1999a, Leung et al 1999). Under general anesthesia with sodium pentobarbital (0.8ml/kg, intravenous injection, Sigma, Chemicals Co., St. Louis MO, USA) and an aseptic technique, one of the knees was approached through an anterolateral skin incision to create the partial patellectomy through a transverse osteotomy conducted between the proximal 2/3 and the distal 1/3 of the patella using an oscillating hand saw (SYNTHES, Mathys AG, Bettlach, Switzerland). The site of osteotomy was determined by measuring the length of patella using a fine caliper. After removal of the distal 1/3 (lower pole) of the patella and its fibrocartilage zone to the patellar tendon, two holes of 0.8mm in diameter evenly spaced were drilled longitudinally through the remaining proximal patella. The patellar tendon was then directly sutured to the proximal patella via the two drilled holes with non-absorbable suture (3/0 Mersilk, ETHICON Ltd. Edinburgh, UK). Figure-of-eight tension band wiring (0.4 mm diameter stainless steel wire, BIOMET LTD, Waterton, UK) was applied around the proximal pole of the patella to the tibial tuberosity to protect possible overstretching the suture for the BTJ reattachment before closing the wound.

The operated knee joint was then immobilized at 90 degrees of flexion for up to 4 weeks using a long leg cast (SCOTCHCAST, Orthopaedic Products 3M, Health Care, St. Paul, MN, USA). Pain relief drug (TEMGESIC, Reckitt & Colman Pharmaceuticals, Hull, UK) was given subcutaneously at a dose of 0.01 mg/kg for three days after the operation. Animals were kept individually in metal cages and fed with standard rabbit diet and water *ad libitum*. This study was approved by the Animal Research Ethics Committee of the Chinese University of Hong Kong (Ref. CUHK4342/03M).

The 3 groups of animals were sacrificed at 6, 12, and 18 weeks after operation respectively, and the BTJ tissues were assessed to investigate the healing over time.

Ultrasound water jet indentation system and data acquisition

A noncontact ultrasound indentation system was developed using water jet as the indenter. A bubbler was used to eject the water jet by controlling the water flow (Figure 1). The diameter of the water ejecting nozzle was 1.94 mm. A 20 MHz focused ultrasound transducer (GE Panametrics, Inc., OH, USA) was fixed with the bubbler, *i.e.,* the water ejector. The focused ultrasound beam could propagate through the bubbler when it was full of water as the coupling medium. The transducer and the bubbler were installed to a 3-D translating device (Parker Hannifin Corporation, Irvine, CA, USA) which was used to adjust the distance between the nozzle and the specimen surface and to perform a 2-D scanning over a tissue specimen. The distances from the specimen surface to the nozzle outlet and the transducer surface were adjusted to be 5.0 mm and 19.5 mm, respectively. A pressure sensor (EPB-C12, Entran Devices, Inc., Fairfield, NJ, USA) was used to measure the water pressure within the water pipe. By calibrating the relationship

between the overall force applied on the platform of the fixation device and the pressure within the water pipe, the pressure applied on the sample surface could be calculated using the water pressure measured by the pressure sensor (Lu et al 2005). A program was developed using Microsoft VC++ to control the 3D translating device and to collect, process and display the ultrasound signals, along with the pressure value, in real time during the indentation process. Thus the movement of the transducer and the acquisition of the radio-frequency (RF) ultrasound signal and pressure data were synchronized. The sampling rate of ultrasound RF data was 500 MHz, and frame rate of A-mode ultrasound was approximately 10 frames per second, which was also the sampling rate of the pressure data. The ultrasound echoes reflected from both the sample surface and bottom under different loading conditions were tracked with multi-windows using a cross-correlation algorithm (Zheng et al 2002) for estimation of the time-shift of each echo signal. The original tissue thickness was calculated from the predetermined speed of sound in the corresponding tissue and the traveling time of sound from the sample surface to its bottom when with an initial water pressure of less than 0.2 kPa, while the subsequent change of thickness, i.e., the deformation of the tissue under indentation was derived from the deflection of the time of flight of the echoes and the speed of sound. The local strain was calculated from the local deformation divided by the corresponding thickness. For the system using 20 MHz ultrasound frequency and 500 MHz sampling rate, the lateral resolution was approximately 0.2 mm, the axial spatial resolution was approximately 0.1 mm, and the axial displacement resolution was approximately 2 μm. The tissue stiffness ratio, defined as the ratio of the pressure applied on the sample surface to the local strain of the sample, was used as an indicator of the elastic modulus

of tissues since it was found well correlated with Young's modulus according to previous phantom studies (Lu et al 2005, 2006).

System validation using tissue-mimicking phantoms

Before the ultrasound water jet indentation system was used to assess the BTJ tissues, its capability of measuring the distribution of tissue elastic properties was validated using six pieces of tissue-mimicking phantoms. Each phantom consisted of a stiff cylindrical inclusion with a diameter of 8 mm inside a homogeneous background (Figure 2). The stiff inclusion cylinders were made of silicones (Rhodia RTV 573, Rhodia Inc. CN7500, Cranbury, NJ, USA). The backgrounds were made of water-agar (Fisher Scientific Co. Fairlawn, NJ, USA) mixture together with a small quantity of *n*-propanol and formaldehyde (Fisher Scientific Co. Fairlawn, NJ, USA). The concentration of agar ranged from 10.0 g/L to 30.0 g/L to produce a background material with different stiffness (Hall et al 1997). In addition, uniform cylindrical samples were also prepared for each phantom material. The Young's moduli of these uniform phantoms were measured using uniaxial compression tests with a material testing machine (Lu et al 2005).

One-dimensional scanning was conducted on each phantom with stiff inclusion along its diametric direction using the 3-D translating device to measure the distribution of the elastic properties. Typically, the phantom was first preloaded with a pressure of 3 kPa and scanned over by the water jet at a moving rate of 1 mm/s and with a step of 0.2 mm to obtain the first 16-mm wide B-scan, i.e. cross-sectional image. It was then scanned over with a pressure of approximately 20 kPa along the identical line for the second B-scan. The deformation of the phantom at each indentation point along the scanned line

was obtained. The ultrasound pulsed echoes reflected from the phantom surface and bottom were tracked for each corresponding measurement site to compose the strain profile. The compressive modulus at each indentation site was calculated from the pressure and the local strain with the assumption that the Poisson's ratios of the inclusion and background materials were the same. The average elastic modulus of the inclusion (E_i) and that of the background (E_b), were compared with those measured from the uniform phantom made from the correspondingly same material using the uniaxial compression tests. The correlation ratio was used to evaluate the capability of the system of measuring the elastic properties.

Measurement of thickness and elastic modulus of BTJ tissues using the ultrasound water jet indentation system

All the BTJ tissue samples were stored at -20^{o}C before use. The sample was first thawed in normal saline solution (0.15 M NaCl) at room temperature 20^{o}C for 1 hour, and then fixed by a fixation device (Figure 1) with the articular surface facing the ultrasound transducer perpendicularly. As shown in Figure 1, a stainless steel device which had two plates was employed to fix the sample at the patella by tightening the two binder bolts. A plastic plate was inserted between the patella and bolts to avoid the sample shifting downwards during indentation loading. The sample was first scanned along the patella-junction-tendon direction with a scan step at 50 μm under a preloading of 2.12 ± 0.07 kPa by the water jet ultrasound indentation system with the flow rate at 1.35 ± 0.07 m/s. The scan line was carefully selected by obtaining the maximal ultrasound reflection echoes from the interface of water/articular surface, usually at the most prominent convex site of

262 the patella. The scan distances were typically 6 mm for a control sample and 5 mm for a
263 postoperative sample. After the first scan was finished, the sample was quickly scanned
264 again along the identical line under a pressure of 135.32 ± 0.36 kPa with the flow rate at
265 7.89 ± 0.01 m/s. We tried to map the elastic modulus of each kind of tissue in the bone-
266 tendon junction complex, including patellar cartilage, fibrocartilage and tendon, therefore,
267 the maximal pressure ensured all kinds of tissue response in the linear elastic region.
268 After many experimental trials, a pressure at 135 kPa was regarded as an appropriate
269 value. A typical control sample is shown in Figure 3a together with its first B-scan of the
270 interested BTJ region (Figure 3b).

271 The ultrasound signals obtained from the first B-scan were analyzed to calculate
272 the tissue original thickness. Three sites from each part, including patellar cartilage,
273 fibrocartilage zone and tendon were selected, and the thickness at each site was
274 calculated from the time of flight of ultrasound signals from the surface to the substrate.
275 The speed of ultrasound in cartilage $c_{cartilage}$ was assumed to be 1636 m/s (Patil et al 2004)
276 and that in tendon c_{tendon} was assumed to be 1580 m/s (Duck 1990). The averaged values
277 calculated from the three sites were used as the thickness value for each tissue part. Then,
278 the thickness change Δh of each selected site under two consequent scans was calculated
279 from the deflection of the flight of time of ultrasound echoes Δt. The elastic modulus was
280 then calculated by the stress applied to the tissue divided by the local strain. As same as
281 the thickness measurement, the averaged values calculated from the three sites were used
282 as the value of elastic modulus for each tissue part.

283

284 *Descriptive histology*

Patella-patellar tendon (PPT) complex was prepared for histological analysis using the established protocols (Qin et al 1999b). Briefly, the PPT complex was fixed in 4% neutrally buffered formalin for 1 day, decalcified with 25% formic acid for 4 weeks, processed using a Histo-center (Histokinette 2000, Reichert-Jung GmbH, Nussloch, Germany) and embedded with paraffin wax using an Embedding Center (Thermolyne Sybron, Dubuque, IA, USA). Mid-sagittal sections at 5μm thickness were prepared using 1130/Biocut microtome (Reichert-Jung GmbH, Nussloch, Germany) and stained with haematoxylin and eosin (H&E). A microscopic image analysis system (Leica Q500MC, Leica Cambridge Ltd, Cambridge, UK) was used to identify the nature of the tissue and its histomorphological features. The fibrocartilage can be classified as uncalcified fibrocartilage which connecting to collagenous tendon and calcified fibrocartilage which connecting to bone. The calcified and uncalcified fibrocartilages are separated by a tidemark that is a continuous border line observable with H&E staining. In addition, the morphology and distribution of cells are also different in the calcified and uncalcified regions. This can be used as an additional clue for the separation of the two regions (Wang et al. 2007, Lu et al. 2008).

Statistical analysis

Data were expressed as mean ± SD. Comparisons of both elastic modulus and thickness of patella, the distal of patella, fibrocartilage and tendon were made by using two-way ANOVA to investigate if the group separation and the sacrificed time would significantly affect these parameters. Then two-way ANOVA was conducted to evaluate the effect of healing time and partial pattelectomy operation. All the statistical analyses were

conducted by using the commercial software SPSS. The significance level was set at $p < 0.05$.

Results

System validation

A typical strain and its corresponding modulus profile across the selected scan line is shown in Figure 4, which was derived from two consequent B-scan images of a tissue-mimicking phantom. Each value in Figure 4 represents the mean of the data of three repeated measurements. Elastic modulus values obtained from the center of the inclusion and background along the scan line (as indicated in Figure 2), were averaged as the elastic moduli of the inclusion E_i and that of the background E_b, respectively. The elastic modulus of each material was compared with that measured from the uniform phantom using the uniaxial compression test (Figure 5). The high correlation coefficient ($r = 0.99$) indicated a very good agreement between them, though some differences between the absolute values were noted.

Thickness and elastic modulus of bone-tendon junction tissues

The values of the elastic modulus and tissue thickness of the patellar cartilage, fibrocartilage and tendon tissue of the control and post-operative samples were listed in Table 1. Since the distal patella was removed during the partial patellectomy operation, the elastic modulus and thickness of patellar cartilage was measured from the remaining proximal patella, as indicated in Figure 3, for a paired comparison between the control

and postoperative samples to study whether the surgery affected the intact cartilage region.

Neither elastic modulus nor thickness showed significant difference among the control samples at different sacrificed time points (all $p > 0.1$), i.e. the sacrificed time had no significant effect on the material properties of the control samples at 95% significance level. In comparison with the control samples, it was found that the elastic moduli of both patellar cartilage and fibrocartilage of the postoperative samples were significantly smaller (with $p < 0.001$ for both comparisons), while that of the tendon tissue was insignificantly larger. In the postoperative sample group, the elastic modulus of the fibrocartilage of the samples harvested at week 18 (100 ± 28 kPa) was significantly higher than those harvested at week 6 (62 ± 21 kPa) with $p = 0.02$ and week 12 (63 ± 31 kPa) with $p = 0.01$, and it was even comparable with the value of the control samples at the same sacrificed time (116 ± 32 kPa). The thickness of the fibrocartilage of the postoperative samples was significantly larger than that of the control samples at all the three time points (with all $p < 0.0001$), while that of the tendon tissues of the postoperative samples was only found significantly larger at week 12 (4.27 ± 0.46 mm v.s. 3.71 ± 0.25 mm) and week 18 (3.93 ± 0.77 mm v.s. 3.58 ± 0.11 mm) with $p < 0.0001$ for both. The thickness values of the tendon tissues were significantly different among the postoperative samples harvested at different time points with $p = 0.03$, but not for the fibroscartilage. There was no significant difference in the elastic modulus of tendon or the thickness of patellar cartilage between the control and postoperative samples.

Histological analysis

353 The normal patella-patellar tendon complex was composed of patella, patellar tendon and
354 fibrocartilage zone connecting the tendon to the bony patella (Figure 6a). Based on H&E
355 stained sections of decalcified postoperative specimens for evaluation of general
356 morphology at the healing interface, scar tissues gradually formed and structurally
357 connected the tendon and patella at the junction gap as the healing time progressed. At
358 postoperative week 6, histological observation revealed tissue integration, the crossing of
359 fibers from tendon into bone, and newly formed bone from the remaining patella after
360 partial patellectomy at healing junction (Figure 6b). Compared with the histomorphology
361 of specimens at week 6, improved tissue integration was found at postoperative week 12,
362 characterized with more outgrowth of trabecular bone from the remaining patella and
363 formation of fibrocarilage layer at the healing junction (Figure 6c). Week 18 samples
364 featured with a regenerated junction morphologically similar to normal patella-patellar
365 tendon (Figure 6d).
366
367 **Discussion**
368 In this study, the healing of bone-tendon junction tissues after partial patellectomy of
369 rabbit models was assessed using a novel noncontact ultrasound water jet indentation
370 system *in situ*. A previous study has suggested that the regeneration of the transitional
371 fibrocartilage could be determined by stiffness measurement (Qin et al 2006). Therefore,
372 determination of the mechanical properties of BTJ tissues would also be useful in trauma
373 and joint repair surgery. In comparison to the currently available indentation systems, the
374 ultrasound water jet indentation system offers the advantage of no direct contact between
375 the device and the sample. During the indentation, the deformation induced by the water

jet compression was small and within the range of linear elastic behaviour of the tissue. The applied load was very small and no structural tissue damage was observed after the experiment according to the histological visualization. Thus, it was assumed that the risk of tissue damage during water jet examination was minimized compared with the conventional contact indentation measurements. However, further analysis of cell viability is required to exclude any cellular damage resulting from the water jet application (Bae et al 2003).

The phantom test in this study proved that the ultrasound water jet indentation system could easily be used for modulus measurement and mapping by obtaining a sequence of B-mode images with the mechanical scanning of the probe under different loadings. By recording the water pressure and ultrasound signal simultaneously at each indentation site during B-scans, the local elastic modulus could be obtained from the indentation force, the local deformation and the original tissue thickness. As demonstrated in the validation test, the average elastic modulus obtained from the modulus profile of each phantom was well correlated with the measured compressive Young's modulus, suggesting that the noncontact ultrasound water jet indentation system could effectively map the elastic modulus of soft tissues by conducting one-dimensional scanning over the tissue under different loadings. However, the elastic modulus obtained by using the current system may be affected by the Poisson's ratio of the phantom materials, the boundary conditions, and the indentation mechanism. In addition, it was suggested that the lateral dimension of the sample should be 3 times larger than the indenter diameter according to the indentation model using cylindrical indenters (Hayes et al 1972, Galbraith and Bryant 1989). This requirement might not always be fulfilled

for the real tissues so that the lateral boundary conditions should be considered in the indentation model. There is still lack of an analytical solution to accurately describe the relationship between the water jet pressure and the deformation during a water jet indentation. Further investigation should be continued to establish a mechanical model of the water jet indentation by considering the effects of Poisson's ratio, the boundary conditions, and the complicated interaction between the water jet and tissue surface, so as to extract the intrinsic material properties of soft tissues more accurately. A water jet with smaller diameter will also be investigated in our future studies to test their feasibility.

It was shown that partial patellectomy operation resulted in a degenerated patellar cartilage and fibrocartilage at the junction, as indicated by the result that the elastic modulus of postoperative samples significantly decreased in comparison with the control samples. The healing of the BTJ junction was evaluated by measuring the elastic modulus and thickness of junction tissues of the postoperative samples at different sacrificing time points. It was found that the elastic modulus of the fibrocartilage of the samples harvested at week 18 was significantly larger than that of the samples harvested at week 6 and week 12. The increase in the elastic modulus during the healing process might result from the increase of the intercross between the increasing proteoglycan contents and collagen matrix. However, no significant difference of tissue thickness was found among the different groups, which was confirmed by the histological analysis. This might be explained that the morphology of BJT can resume to the intact status quickly after surgery. However, it takes longer time for tissue to gain its function, which means the mechanical properties for the case of fibrocartilage, as its main function is to provide a mechanical link between patella and tendon. The result of histological analysis revealed

422 that the calcified region under the fibrocartilage increased as time going. This might
423 indirectly indicate that the tissue became stiffer during the healing process.

424 Tensile failure tests are commonly used to quantify the strength of bone-tendon
425 junction (Leung et al. 2002). However, due to the fact that failure occurred at bone-
426 tendon junction either at osteotomy line for samples at early healing or at new bone and
427 residual bone in samples with longer healing time for testing the BTJ healing complex in
428 our previous partial patellectomy model (Leung et al. 2002), we were not able to obtain
429 information on tendon mechanical properties for a correlation study. As histological
430 evaluations required intact specimens so we did not have tensile testing data generated
431 directly from these samples used for ultrasound and histological tests. However, it would
432 be possible to include the tensile testing for samples after ultrasound indentation tests in
433 our future studies although the failure load may not be delineated either for tendon or
434 new bone formation at the bone-tendon healing junction. Since the mechanical properties
435 of BTJ are highly nonlinear, to decide a suitable loading condition is a challenge. If the
436 load is low, the tendon may dominant the measured mechanical properties. If the load is
437 too high, there is a risk of failure. Nevertheless, tensile testing is an appropriate approach
438 to validate the results of the water jet indentation test reported in this study, in relation to
439 the function of bone-tendon junction. If the results can be verified, water jet ultrasound
440 indentation may provide a potential nondestructive method for the evaluation of the BTJ
441 complex.

442 In this study, we used a group of rabbit without surgery as a control and
443 demonstrated the significant difference of tissue stiffness between the control and partial
444 patellectomy groups. In general, the contralateral sites might be more preferred as a

control as they are from the same rabbit. However, our initial concern was the effect of the surgery to the tissues of the contralateral side could not be known. If we use the contralateral side for comparison, the interpretation of the result would also be complicated. Nevertheless, this issue can be further investigated in future studies.

In summary, our novel water jet indentation was successfully used in this study to measure the material properties of BTJ tissues of rabbit models after the phantom test and validity test were conducted. Based on further modifications and by taking into account the effects of sample boundary condition and interaction between the sample and water jet, etc, the current water jet indentation system could provide a useful method to assess the BTJ healing process after trauma and reconstructive surgeries, considering the finding that mechanical properties directly related to the healing status. In comparison with histology, the current method can provide tissue thickness and elasticity nondestructively *in situ* and with no need to wait for the long time required by histology. It can be predicted that the measurement in vivo would be more complicated because of the nonlinearity, viscoelasticity, and inhomogeneity of biological tissues. We are devoted to developing a theoretical solution for the interaction between water jet and tissues. With such a solution, we can better understand whether different factors affecting the pressure-deformation relationship will compensate with each other or not.

Acknowledgements

This work was partially supported by The Hong Kong Polytechnic University (J-BB69), the Research Grants Council of Hong Kong (PolyU 5245/03E, PolyU 5318/05E,

467 and CUHK4342/03M), Guangdong Natural and Science Foundation (No.
468 8451806001001751) and Youth Fund of Shenzhen University (No. 200843).
469

References

Adam C, Eckstein F, Milz S, Schulte E, Becker C and Putz R. The distribution of cartilage thickness in the knee-joints of old-aged individuals - measurement by A-mode ultrasound. *Clin. Biomech.* 1998; 13:1-10.

Appleyard RC, Swain MV, Khanna S, Murrell GA. The accuracy and reliability of a novel handheld dynamic indentation probe for analysing articular cartilage. *Phys. Med. Biol.* 2001; 46:541–50.

Arokoski J, Jurvelin J, Kiviranta I, Tammi M and Helminen HJ. Softening of the lateral condyle aricular-cartilage in the canine knee-joint after long-distance (up to 40KM/day) running training lasting one-year. *Int. J. Sports Med.* 1994; 15:254-60

Arokoski JPA, Hyttinen MM, Helminen HJ and Jurvelin JS. Biomechanical and structural characteristics of canine femoral and tibial cartilage. *J. Biomed. Mater. Res.* 1999: 48:99-107

Athanasiou KA, Agarwal A, Muffoletto A, Dzida FJ, Constantinides G and Clem M. Biomechanical properties of hip cartilage in experimental animal-models. *Clin. Orthop. Res*. 1995; 316:254-66

Athanasiou KA, Fleischli JG, Bosma J, Laughlin TJ, Zhu CF, Agrawal CM and Lavery LA. Effects of diabetes mellitus on the biomechanical properties of human ankle cartilage. *Clin. Orthop. Res*. 1999; 368:182-9

Bae WC, Lewis CW, Sah RL. Intra-tissue strain distribution in normal human cartilage during clinical indentation testing. *Trans. Orthop. Res. Soc.* 2003; 28:1

Benjamin M, Ralphs JR. Fibrocartilage in tendon and ligaments: An adaptation to compressive load. *J Anat* 1998; 193:481-94

493 Buckwalter JA. Activities vs rest in the treatment of bone, soft tissue and joint injuries.
494 *Iowa. Orthop. J.* 1995; 15:29-42
495 Duck FA. Physical properties of tissue: a comprehensive reference book. London:
496 Academic Press, 1990
497 Gao JZ and Messner K. Quantitative comparison of soft tissue-bone interface at chondral
498 ligament insertion in the rabbit knee joint. *J. Anat.* 1996; 188:367-73.
499 Gao L, Parker KJ, Lerner RM and Levinson SF. Imaging of the elastic properties of
500 tissue-a review. *Ultrasound Med. Biol*. 1996; 22:959-77
501 Greenleaf JF, Fatemi M and Insana M. Selected methods for imaging elastic properties of
502 biological tissues. *Annu. Rev. Biomed. Eng.* 2003; 5:57-8.
503 Haider MA and Holmes MH. A mathematical approximation for the solution of a static
504 indentation test. *J. Biomech.* 1997; 30:747-51
505 Hall TJ, Bilgen M, Insana MF and Krouskop TA. Phantom materials for elastography.
506 *IEEE Trans. Ultrason. Ferroelectr. Freq. Control.* 1997; 44:1355-65
507 Han LH, Noble JA and Burcher M. A novel ultrasound indentation system for measuring
508 biomechanical properties of in vivo soft tissue. *Ultrasound Med. Biol.* 2003; 29:813-
509 23
510 Hayes WC, Keer LM, Herrmann G and Mockros LF. A mathematical analysis for
511 indentation tests of articular cartilage. *J. Biomech*. 1972; 5:541-51
512 Hori RY and Mockros LF. Indentation tests of human articular-cartilage. *J. Biomech*.
513 1976; 9:259-68

514 Hung LK, Lee SY, Leung KS, Chan KM and Nicholl LA. Partial patellectomy for
515 patellar fracture: tension and band wiring and early mobilization. *J. Orthop. Trauma*
516 1993; 7:252-260
517 Hsu TC, Wang CL, Shau YW, Tang FT, Li KL and Chen CY. Altered heel-pad
518 mechanical properties in patients with Type 2 diabetes mellitus. *Diabet Med.* 2000;
519 17:854-9
520 Hsu TC, Wang CL, Tsai WC, Kuo JK and Tang FT. Comparison of the mechanical
521 properties of the heel pad between young and elderly adults. *Arch. Phys. Med.*
522 *Rehabil.* 1998; 79:1101-4
523 Huang YP, Zheng YP and Leung SF. Quasilinear viscoelastic parameters of neck tissues
524 with fibrosis induced by radiotherapy. *Clin. Biomech.* 2005; 20:145-54.
525 Jurvelin J, Kiviranta I, Saamanen AM, Tammi M and Helminen HJ. Indentation stiffness
526 of young canine knee articular-cartilage – influence of strenuous joint loading. *J.*
527 *Biomech*. 1990; 23:1239-46
528 Jurvelin JS, Rasanen T, Kolmonen P and Lyyra T. Comparison of optical, needle probe
529 and ultrasonic techniques for the measurement of articular-cartilage thickness. *J.*
530 *Biomech.* 1995; 28:231-5.
531 Kawchuk GN and Elliott PD. Validation of displacement measurements obtained from
532 ultrasonic images during indentation testing. *Ultrasound Med. Biol.* 1998; 24: 105-11
533 Kawchuk GN, Fauvel OR and Dmowski J. Ultrasound indentation: a procedure for the
534 noninvasive quantification of force-displacement properties of the lumber spine. *J.*
535 *Manipulative Physiol. Ther.* 2001; 24:149-56

536 Kawchuk GN, Fauvel OR and Dmowski J. Ultrasonic quantification of osseous
537 displacements resulting from skin surface indentation loading of bovine para-spinal
538 tissue. *Clin. Biomech.* 2000; 15:228-33
539 Kempson GE, Freeman MAR and Swanson SAV. The determination of a creep modulus
540 for articular cartilage from indentation tests on human femoral head. *J. Biomech.*
541 1971; 4: 239-50
542 Laasanen MS, Toyras J, Hirvonen J, Saarakkala S, Korhonen RK, Nieminen MT,
543 Kiviranta I and Jurvelin JS. Novel mechano-acoustic technique and instrument for
544 diagnosis of cartilage degeneration. *Physiol. Meas.* 2002; 23:491-503
545 Laasanen MS, Saarakkala S, Toyras J, Hirvonen J, Rieppo J, Korhonen RK and Jurvelin
546 JS. Ultrasound indentation of bovine knee articular cartilage in situ. *J. Biomech.*
547 2003; 36:1259-67
548 Leung KS, Qin L, Fu LK and Chan CW. A comparative study of bone to bone repair and
549 bone to tendon healing in patella-patellar tendon complex in rabbits. *Clin. Biomech.*
550 *(Bristol Avon)* 2002; 17:594-602
551 Leung KS, Qin L, Leung MCT, Fu LLK and Chan CW. Partial patellectomy induces a
552 decrease in the proteoglycan content in the remaining patellar articular cartilage. An
553 experimental study in rabbits. *J. Clin. Exper. Rheumatol.* 1999; 17:597-600
554 Leung SF, Zheng YP, Choi CYK, Mak SSS, Chiu SKW, Zee B and Mak AFT.
555 Quantitative measurement of post-irradiation neck fibrosis based on the Young
556 modulus: description of a new method and clinical results. *Cancer* 2002; 95:656-62

557 Lu HB, Qin L, Fok PK, Cheung WH, Lee KM, Guo X, Wong WN and Leung KS. Low
558 Intensity Pulsed Ultrasound Accelerates Bone-Tendon-Junction Healing- A Partial
559 Patellectomy Model in Rabbits, *J. Am. Sports. Med.* 2006; 34:1287-96
560 Lu HB, Qin L, Cheung WH, Wong WN and Leung KS. Low-Intensity Pulsed Ultrasound
561 Accelerated Bone-Tendon Junction Healing through Regulation of Vascular
562 Endothelial Growth Factor Expression and Cartilage Formation. *Ultrasound Med.*
563 *Biol.* 2008; 34:1248-60.
564 Lu MH, Zheng YP and Huang QH. A novel method to obtain modulus image of soft
565 tissues using water jet indentation. *IEEE Trans. Biomed. Eng*. 2006; 54:114-21
566 Lu MH, Zheng YP and Huang QH. A Novel non-contact ultrasound indentation system
567 for measurement of tissue material properties using water jet compression.
568 *Ultrasound Med. Biol*. 2005; 31:817-26.
569 Lu MH, Zheng YP, Huang QH, Ling HY, Wang Q, Bridal SL, Qin L and Mak AFT.
570 Noncontact evaluation of articular cartilage degeneration using a novel ultrasound
571 water jet indentation system. *Ann. Biomed. Eng.* 2009; 37:164-75.
572 Lyyra T, Jurvelin J, Pitkanen P, Vaatainen U and Kiviranta I. Indentation instrument for
573 the measurement of cartilage stiffness under arthroscopic control. *Med. Eng. Phys*.
574 1995; 17:395-9
575 Mak AF, Lai WM and Mow VC. Biphasic indentation of articular-cartilage .1. theoretical
576 -analysis. *J. Biomech*. 1987; 20:703-14
577 Mow VC, Gibbs MC, Lai WM, Zhu WB and Athanasiou KA. Biphasic indentation of
578 articular-cartilage .2. a numberical algorithm and an experimental-study. *J. Biomech*.
579 1989; 22:853-61

580 Nebelung W, Becker R, Urbach D, Ropke M and Roessner A. Histological findings of
581 tendon-bone healing following anterior cruciate ligament reconstruction with
582 hamstring graft. *Arch. Orthop. Trauma Surg.* 2003; 123:158-63
583 Newton PM, Mow VC, Gardner TR, Buckwalter JA and Albright JP. The effect of
584 lifelong exercise on canine articular cartilage. *Am. J. Sports Med*. 1997; 25:282-7
585 Neiderauer MQ, Cristante S, Neierauer GM, Wilkes RP, Singh SM, Messina DF, Walter
586 MA, Boyan BD, DeLee JC and Neiderauer GG. A novel instrument for
587 quantitatively measuring the stiffness of articular cartilage. *Trans. Orthop. Res. Soc*.
588 1998; 23:905
589 Neiderauer GG, Neierauer GM, Cullen LC, Athanasiou KA, Thomas JB and Niederauer
590 MQ. Correlation of cartilage stiffness to thicknes and level of degeneration using a
591 handheld indentatio probe. *Ann. Biomed. Eng.* 2004; 32:352-9
592 Nummi J. Fracture of the patella: a clinical study of 707 patellar fractures. *Ann. Chir.*
593 *Gynaecol.* 1971; 60:179-85
594 Ophir J, Ce´spedes EI, Ponnekanti H, Yazdi Y and Li X. Elastography: a quantitative
595 method for imaging the elasticity of biological tissues. *Ultrasound Imaging* 1991;
596 13:111–34
597 Ophir J, Kallel F, Varghese T, Bertrand M, Ce´spedes I, Ponnekanti H. Elastography: a
598 systems approach. *International J. Imaging Sys. Tech.* 1997; 8:89–103
599 Patil SG, Zheng YP and Shi J. Measurement of depth-dependence and anisotropy of
600 ultrasound speed of bovine articular cartilage in vitro. *Ultrasound Med. Biol*. 2004;
601 30:953-63

602 Qin L, Appell HJ, Chan KM and Maffulli N. Electrical stimulation prevents
603 immobilization atrophy skeletal muscle of rabbits. *Arch. Phys. Med. Rehabil*. 1997;
604 78:512-7
605 Qin L, Lu HB, Fok PK, Cheung WC, Zheng YP, KM Lee, Leung KS. Low intensity
606 pulsed ultrasound accelerates osteogenesis at bone-tendon junction healing junction.
607 *Ultrasound Med. Biol.* 2006a; 32:1905-11
608 Qin L, Fok P, Lu H, Shi S, Leng Y and Leung K. Low intensity pulsed ultrasound
609 increases the matrix hardness of the healing tissues at bone-tendon insertion- a
610 partial patellectomy model in rabbits. *Clin. Biomech.* 2006b; 21:387-94
611 Qin L, Leung KS, Chan CW, Fu LK and Rosier R. Enlargement of remaining patella
612 partial patellectomy in rabbits. *Med. Sci. Sports Exerc.* 1999a; 31 502-6
613 Qin L, Mak AFT, Cheng CW, Hung LK and Chan KM. Histomorphological study on
614 pattern of fluid movement in cortical bone in goats. *Anat. Rec.* 1999b; 255:380-7
615 Sakamoto M, Li GA, Hara T and Chao EYS. A new method for theoretical analysis of
616 static indentation test. *J. Biomech.* 1996; 29:679-85
617 Saltzman CL, Goulet JA, McClellan RT, Schneider LA, Matthews LS and Michgan AA.
618 Results of treatment of displaced patellar fracture by partial patellectomy. *J. Bone*
619 *Joint Surg. (Am.)* 1990; 72:1279-85
620 Setton LA, Elliott DM and Mow VC. Altered mechanics of cartilage with osteoarthritis:
621 human osteoarthritis and an experimental model of joint degeneration. *Osteoarthritis*
622 *cartilage* 1999; 7:2-14

623 Shepherd DET and Seedhom BB. Technique for measuring the compressive modulus of
624 articular cartilage under physiological loading rates with preliminary results. *J. Eng.*
625 *Med*. 1997; 211:155-65
626 Suh JK and Spilker RL. Indentation analysis of biphasic articular-cartilage – nonlinear
627 phenomena under finite deformation. *J.Biomech.Eng.– T. ASME* 1994; 116:1-9
628 Suh JKF, Youn I and Fu FH. An in situ calibration of an ultrasound transducer: a
629 potential application for an ultrasonic indentation test of articular cartilage. *J.*
630 *Biomech*. 2001; 34:1347-53
631 Svensson WE and Amiras D. Ultrasound elasticity imaging. *Breast Cancer Online*. 2006;
632 9:1-7.
633 Waters NE. The indentation of thin rubber sheets by spherical indentors. *Brit. J. Appl.*
634 *Phys*. 1965; 16:557-63
635 Wilson LS and Robinson DE. Ultrasonic measurement of small displacements and
636 deformations of tissue. *Ultrason. Imaging*. 1982; 4:71–82
637 Wilson LS, Robinson DE and Dadd MJ. Elastography-the movement begins. *Phys. Med.*
638 *Biol.* 2000; 45:1409-21.
639 Wang W, Chen HH, Yang XH, Xu G, Chan KM and Qin L. Postoperative programmed
640 muscle tension augmented osteotendinous junction repair. *Int. J. Sports Med.* 2007;
641 28:691-6
642 Yang F. Thickness effect on the indentation of an elastic layer. *Mat. Sci. Eng. A*. 2003;
643 358:226-32
644 Yu W, Li YB, Lim NY, Lu MH, Zheng YP, and Fan JT. Softness measurements for
645 open-cell foam materials and human soft tissue. *Meas. Sci. Tech.* 2006; 17:1785-91.

Yu WP and Blanchard JP. An elastic-plastic indentation model and its solutions. *J. Mater. Res.* 1996; 11:2358-67

Zhang M, Zheng YP and Mak AFT. Estimating the effective Young's modulus of soft tissues from indentation tests - nonlinear finite element analysis of effects of friction and large deformation. *Med. Eng. Phys.* 1997; 19:512-7

Zheng YP and AFT Mak. An ultrasound indentation system for biomechanical properties assessment of soft tissues in-vivo. *IEEE Trans. Biomed. Eng*. 1996; 43:912-8

Zheng YP, Choi YKC, Wong K, Chan S and Mak AFT. Biomechanical assessment of plantar foot tissue in diabetic patients using an ultrasound indentation system. *Ultrasound Med. Biol.* 2000a; 26:451-6

Zheng YP, Leung SF and Mak AFT. Assessment of neck tissue fibrosis using an ultrasound palpation system: A feasibility study. *Med. Biol. Eng. Comput.* 2000b; 38:497-502

Zheng YP, Li ZM, Choi APC, Lu MH, Chen X, and Huang QH. Ultrasound palpation sensor for tissue thickness and elasticity measurement - assessment of transverse carpal ligament. *Ultrasonics*. 2006; 44:e313-7.

Zheng YP and Mak AFT. Extraction of quasilinear viscoelastic parameters for lower limb soft tissues from manual indentation experiment. *J. Biomech. Eng.- T. ASME* 1999a; 121:330-9

Zheng YP and Mak AFT. Effective elastic properties for lower limb soft tissues from manual indentation experiment. *IEEE T. Rehabil. Eng.* 1999b; 7:257-67

667 Zheng YP, Mak AFT, Lau KP and Qin L. An ultrasonic measurement for in vitro depth-
668 dependent equilibrium strains of articular cartilage in compression. *Phys. Med. Biol.*
669 2002; 47:3165-80
670
671

Figure Captions:

Figure 1. Diagram of the ultrasound indentation system using the water jet compression. The water jet was used as an indenter and focused high-frequency ultrasound was employed to monitor the deformation of the soft tissue. The 3D translating device facilitated the system to conduct B-scans over tissue surface. By applying different pressures for B-scan sequences, the distribution of the elastic modulus was obtained with the recorded pressure, deformation and tissue thickness. The fixation of the specimen in the holder was elaborated with the views from different angles.

Figure 2. A picture of the cylindrical phantom used for the system validation. The inclusion with a diameter of 8 mm was made of different silicones and the background was made of agar-water mixture with different concentrations. The dark line in the center indicates the 16-mm wide B-scan line. The data measured from the region along the line, marked as “A” and “B”, were averaged to represent the values of the inclusion and background materials, respectively.

Figure 3. (a) A typical control sample, i.e. intact BTJ tissue, including the patella, fibrocartilage and tendon. The dashed rectangle indicates the region of interest (ROI). (b) The B-scan obtained from the ROI indicated in (a). The patella, fibrocartilage and tendon tissues could be identified from the ultrasound B-scan.

Figure 4. Typical strain (a) and its corresponding modulus profile (b) across the selected scan line of a tissue-mimicking phantom derived from two consequent B-scan images.

695 The error bar indicates the strain and modulus variation of three repeated measurements.
696 The scan distance means the horizontal distance of a measurement region with reference
697 to the left side of the image.
698
699 Figure 5. The correlation between the moduli of the phantom materials determined using
700 the water jet indentation and those measured using the uniaxial compression. The error
701 bar indicates the standard deviation of the measurements.
702
703 Figure 6 Micrographs (H&E staining, magnification: x16) of the midsagittal sections of
704 the patella-patellar tendon (PPT) complex, normal (a), healing PPT complexes after
705 partial patellectomy at postoperative week 6 (b), week 12 (c) and week 18 (d). (a) Normal
706 PPT complex is composed of patella, patellar tendon and fibrocartilage zone connecting
707 the tendon to the bony patella. (b) At postoperative week 6, histological observation
708 reveals tissue integration and newly formed bone from the remaining patella after partial
709 patellectomy at healing junction. (c) Improved tissue integration is found, characterized
710 with more outgrowth of trabecular bone from the remaining patella and formation of
711 fibrocarilage layer at the healing junction at postoperative week 12. (d) Week 18 samples
712 are characterized with a regenerated junction morphologically similar to normal patella-
713 patellar tendon. The dashed line in each figure indicates approximate location of the
714 surgical line for removing the bone. The dotted lines indicate the contour of the patellar
715 bone (a) and newly formed bone (b-d)

Table 1. The elastic modulus of the BTJ tissues measured using the ultrasound water jet indentation system.

	Week 6		Week 12		Week 18	
Elastic modulus (kPa)	Control	Postoperative	Control	Postoperative	Control	Postoperative
Patella Cartilage[*]	490 ± 148	230 ± 98	544 ± 34	262 ± 131	479 ± 147	265 ± 41
Fibrocartilage[*]	107 ± 30	62 ± 22	114 ± 6	63 ± 31	116 ± 32	100 ± 28[#]
Tendon	69 ± 21	81 ± 55	76 ± 17	93 ± 1	58 ± 16	76 ± 15
Thickness (mm)						
Patella Cartilage	0.56 ± 0.10	0.83 ± 0.11	0.56 ± 0.16	0.52 ± 0.08	0.49 ± 0.39	0.60 ± 0.08
Fibrocartilage[*]	0.26 ± 0.04	0.67 ± 0.28	0.21 ± 0.01	0.56 ± 0.35	0.30 ± 0.11	0.69 ± 0.15
Tendon[**]	3.76 ± 0.45	3.68 ± 1.44	3.71 ± 0.25	4.27 ± 0.46	3.58 ± 0.11	3.93 ± 0.77

[*] $P < 0.01$, the effect of operation factor (two-way ANOVA).

[**] $P < 0.05$, the effect of operation factor (two-way ANOVA).

[#] $P < 0.05$, the effect of healing time at the postoperative group.

Figure 1
Click here to download high resolution image

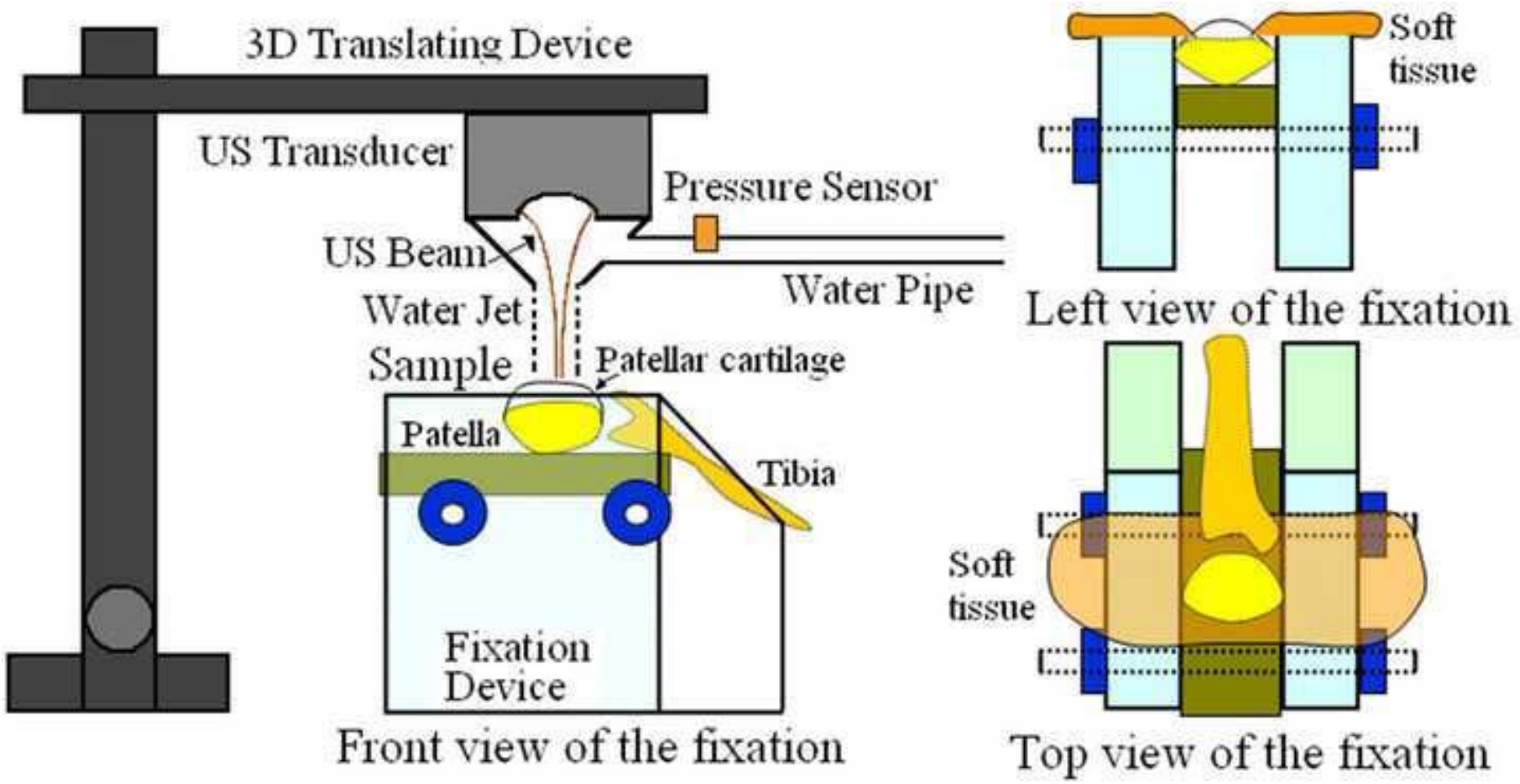

Figure 6
Click here to download high resolution image

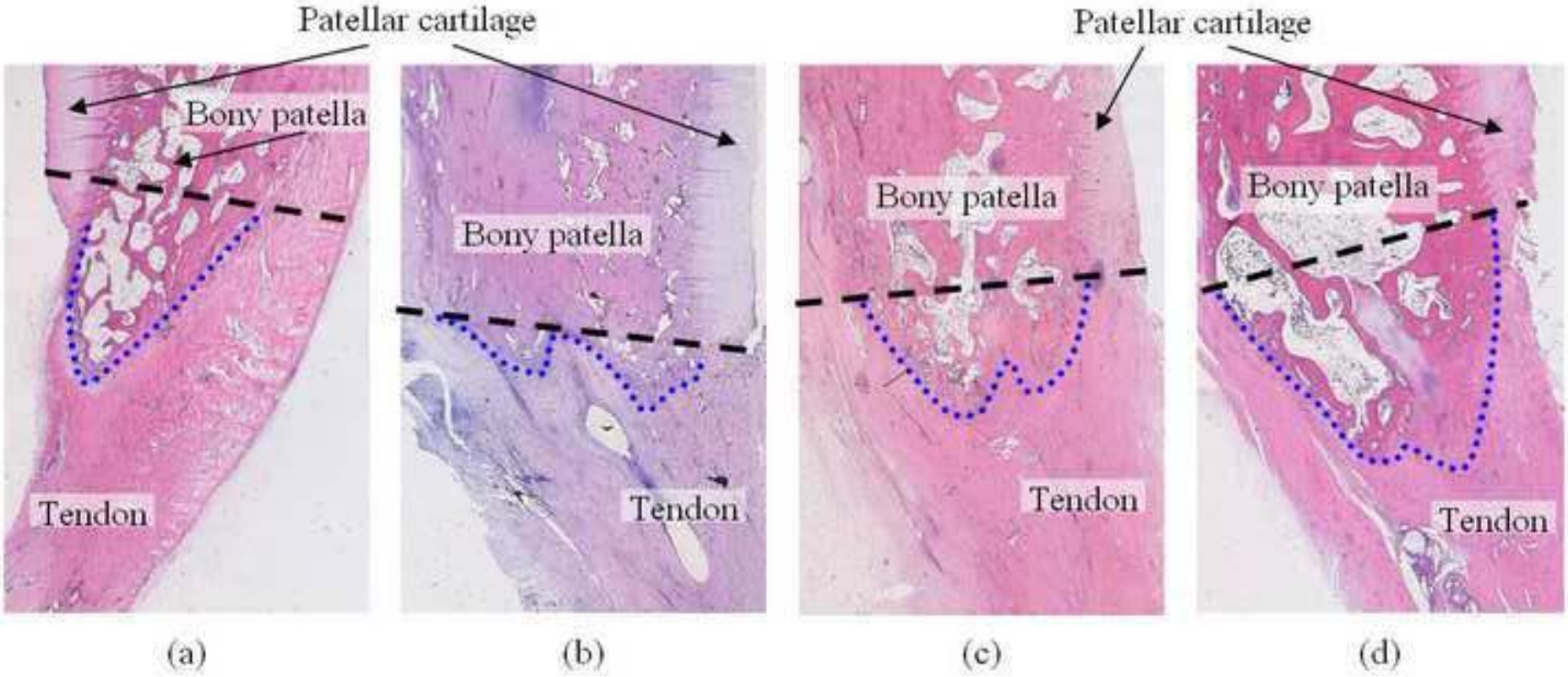

Figure 2
Click here to download high resolution image

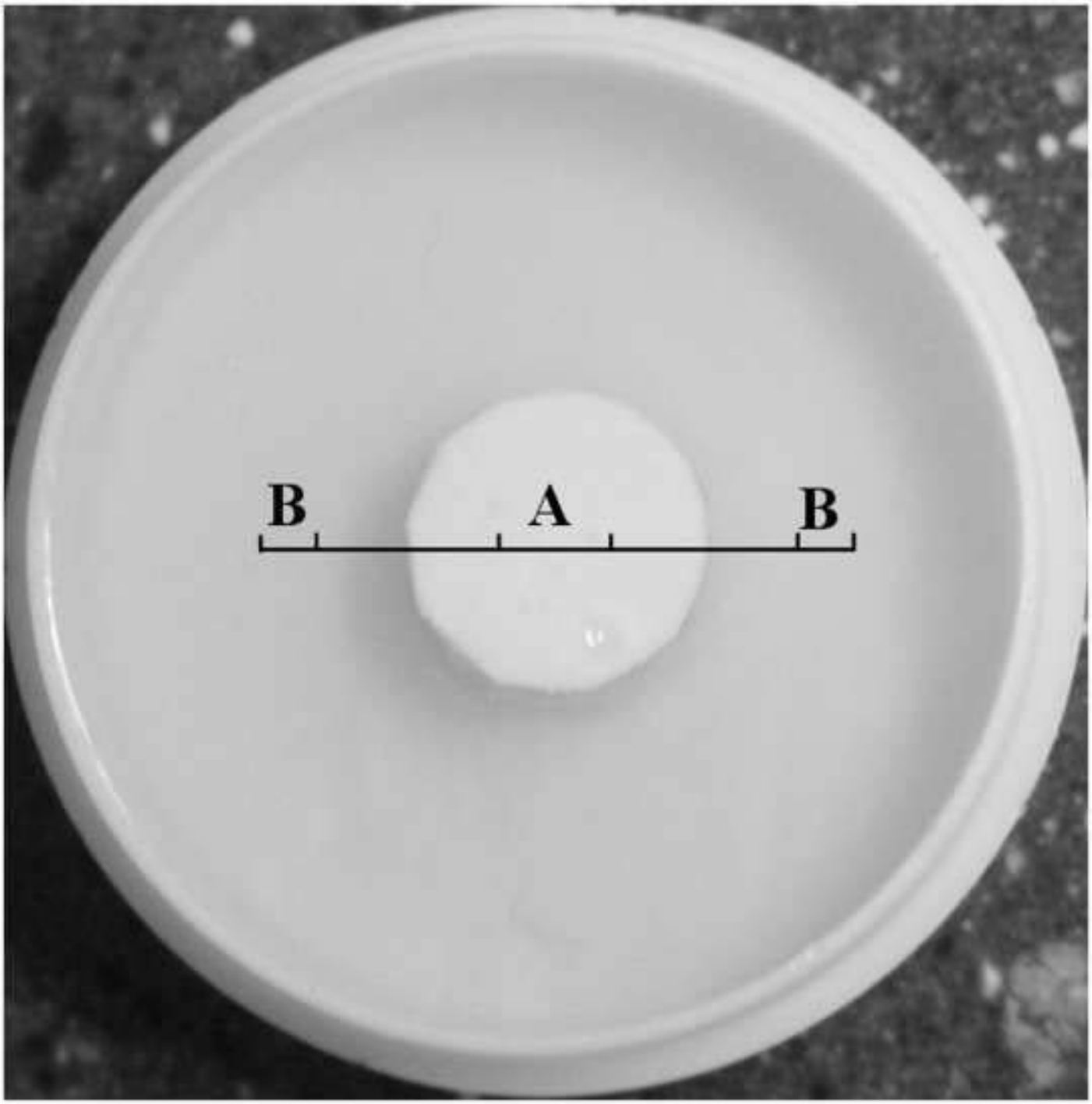

Figure 3a
Click here to download high resolution image

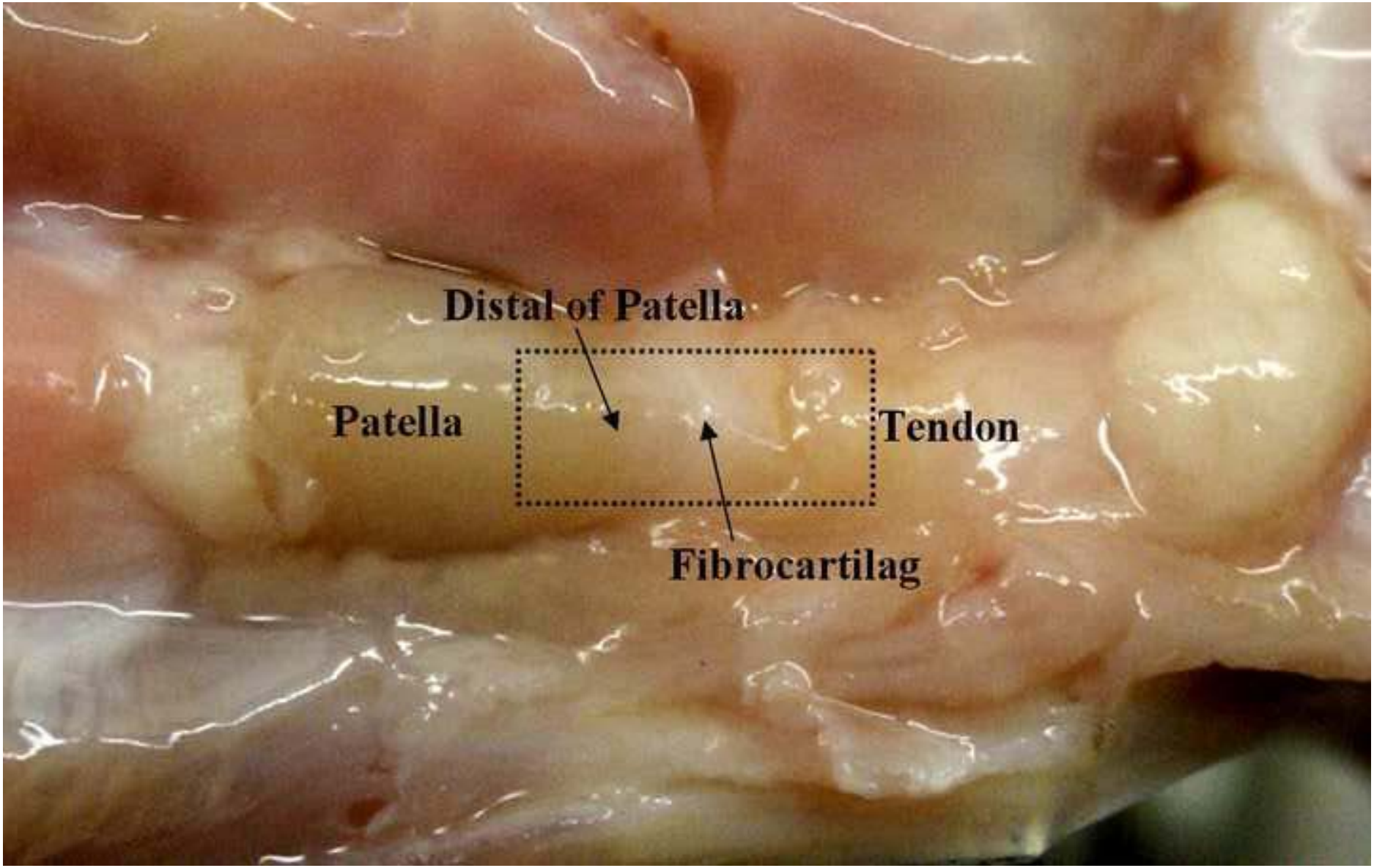

Figure 3b
Click here to download high resolution image

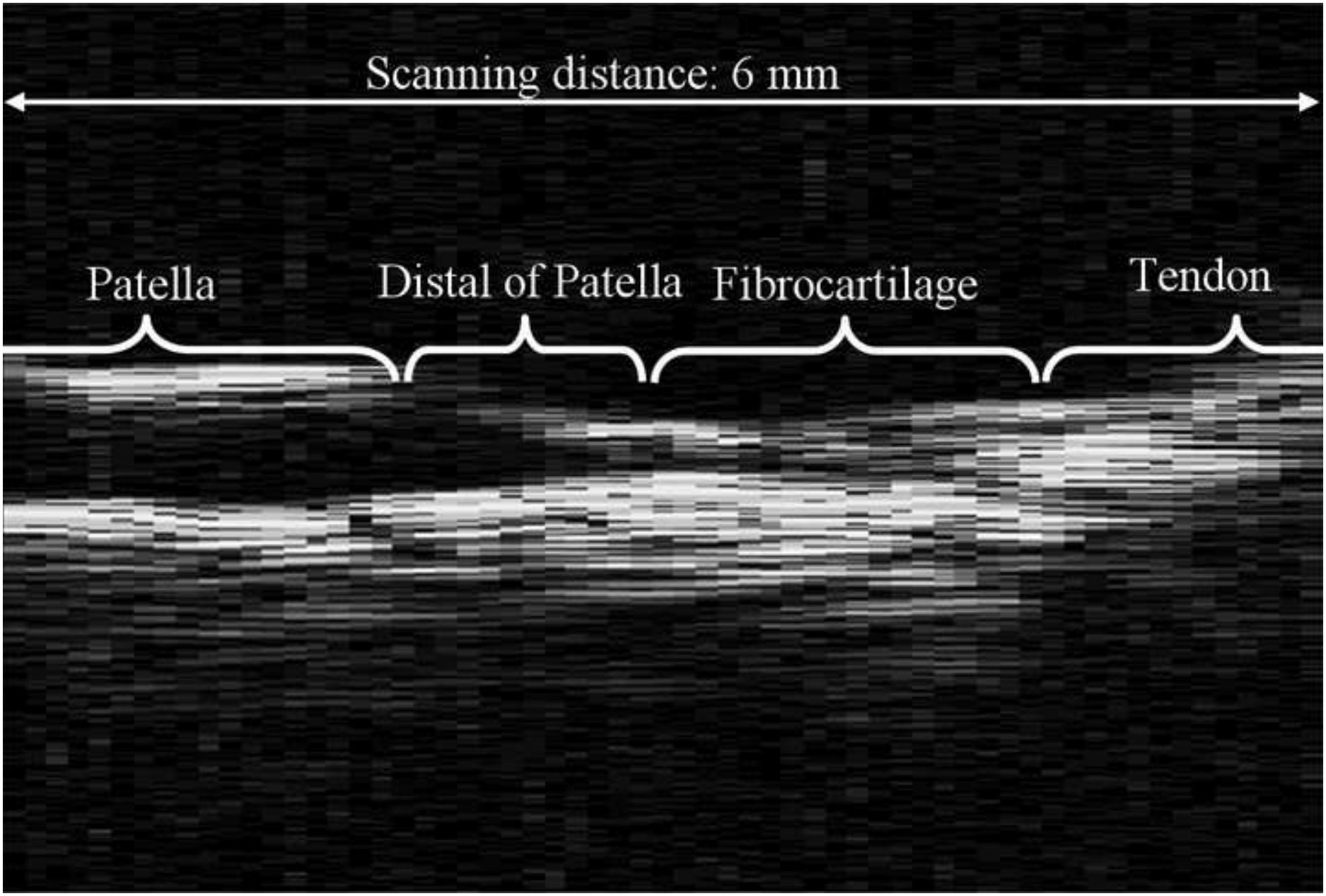

Figure 4a
Click here to download high resolution image

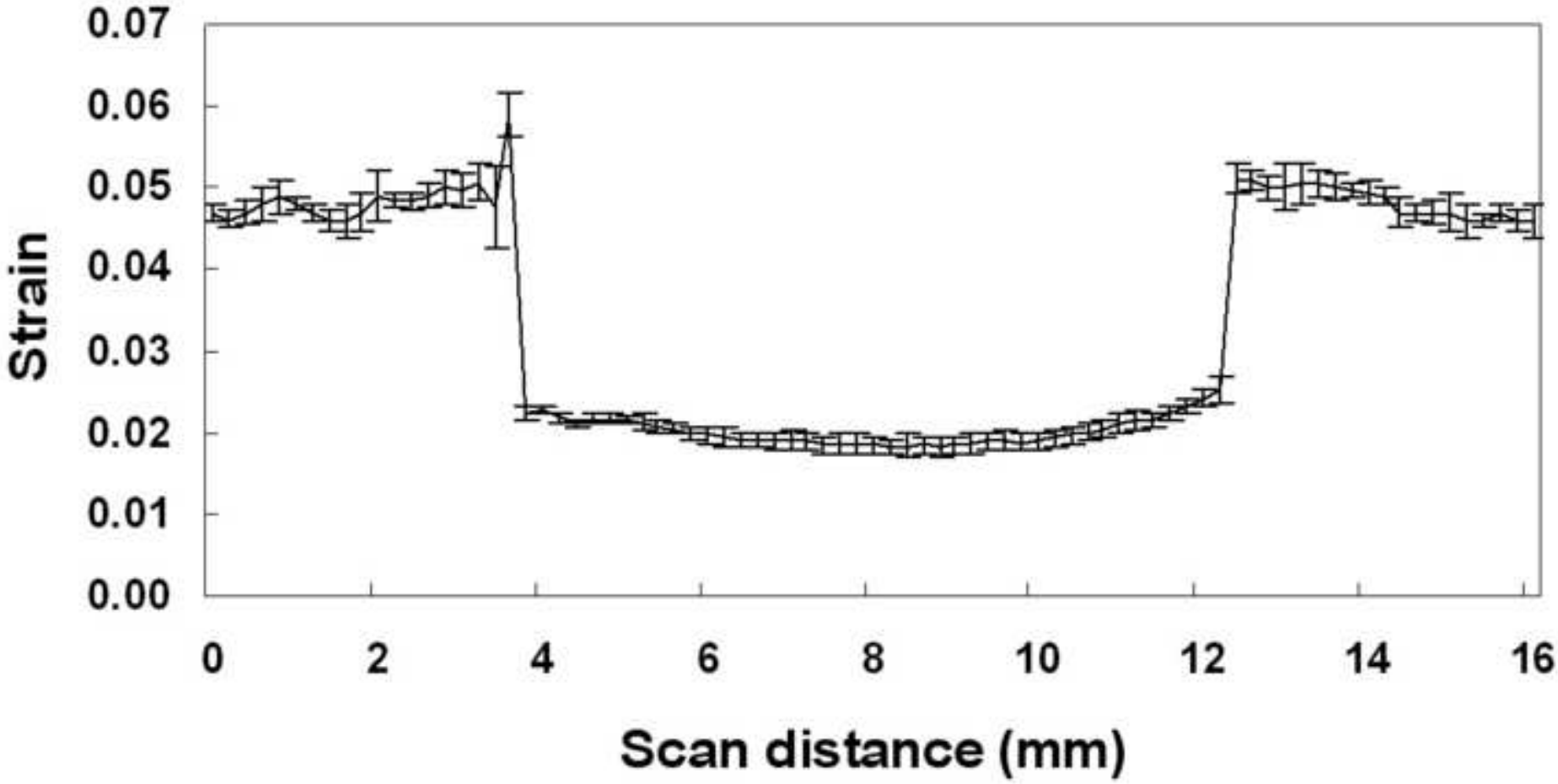

Figure 4b
Click here to download high resolution image

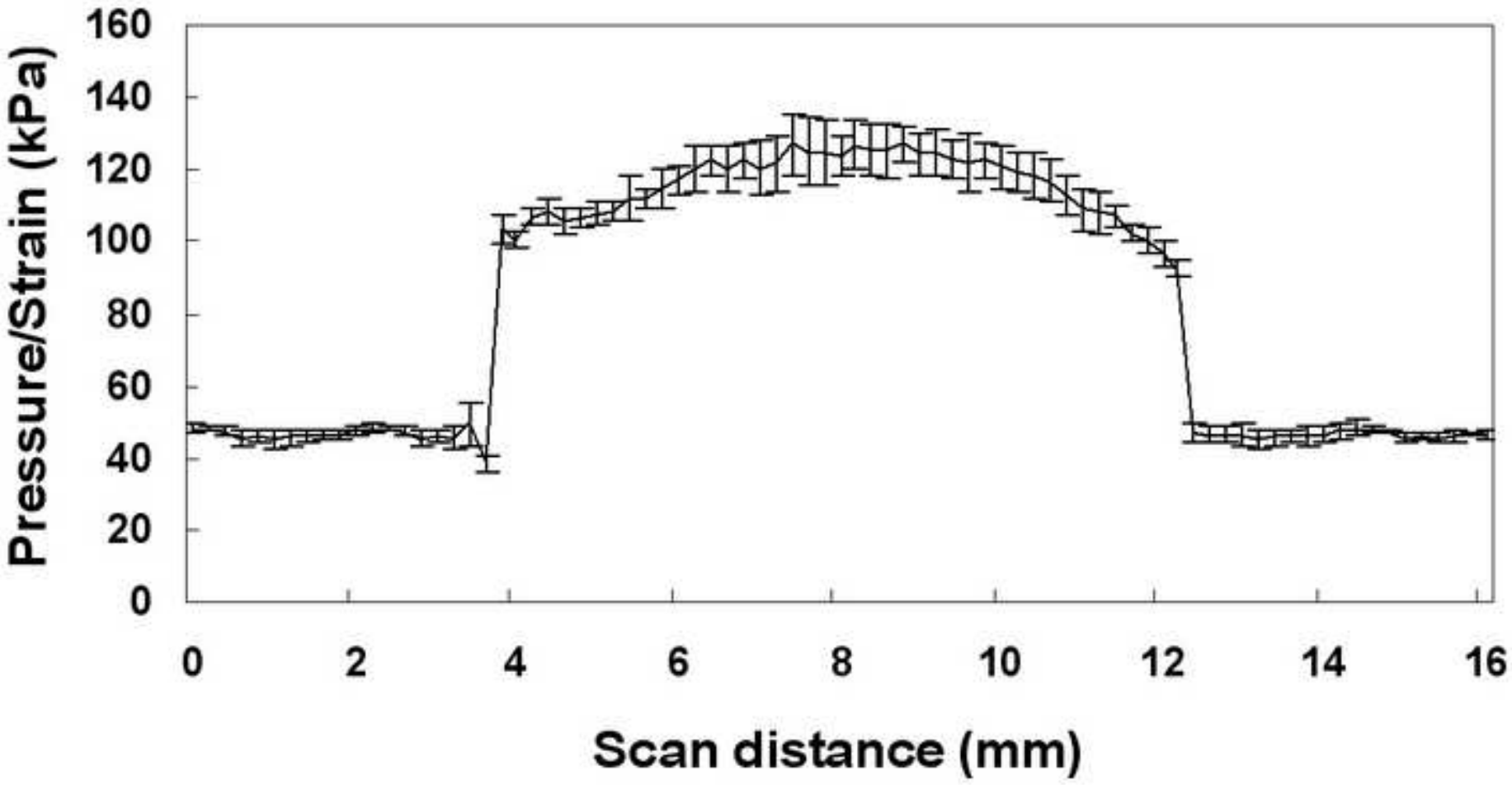

Figure 5
Click here to download high resolution image